Charge-transfer model for carbonaceous electrodes in polar environments

Lars Pastewka,[1] Tommi T. Järvi,[1,*] Leonhard Mayrhofer,[1] and Michael Moseler[1,2,3]
[1]*Fraunhofer-Institut für Werkstoffmechanik IWM, Wöhlerstrasse 11, D-79108 Freiburg, Germany*
[2]*Freiburger Materialforschungszentrum, Stefan-Meier-Strasse 21, D-79104 Freiburg, Germany*
[3]*Albert-Ludwigs Universität, Physikalisches Institut, Hermann-Herder-Strasse 3, D-79104 Freiburg, Germany*
(Received 29 October 2010; revised manuscript received 24 January 2011; published 14 April 2011)

A realistic treatment of metallic and semimetallic systems in polar environments requires an explicit treatment of charges induced into the metallic surface. In classical electrostatics, a metallic surface is properly described if the electric field perpendicular to the surface vanishes. For nanoscale materials, however, charge screening is imperfect because the nanoscale object's surface density of states is finite. Here, we demonstrate that from quantum considerations a classical mean-field charge-transfer model can be extracted, which is demonstrated for graphene and metallic single-wall carbon nanotubes. The model is easily parametrized and gives an approximate description of the binding of point charges on these structures. Potential applications include the modeling of charged or fully biased nanoscale systems in a polar environment, which we demonstrate by simulating a water droplet in a biased graphene nanocapacitor at a fraction of the computational cost of a fully quantum-mechanical treatment.

DOI: 10.1103/PhysRevB.83.165418 PACS number(s): 82.45.Yz, 82.45.Fk, 81.05.U−, 73.61.Wp

I. INTRODUCTION

Carbonaceous materials are traditionally used for electrodes. Common supercapacitors, for example, use activated carbon as the electrode material because of its large surface area and chemical inertness.[1] Even higher capacities are expected once the technological obstacles inhibiting the use of the recently discovered carbon allotropes, carbon nanotubes (CNTs),[2] and graphene[3] are overcome. CNTs, for example, exhibit a huge surface area because of their one-dimensional high aspect-ratio structure. Also graphenes have been shown to yield extraordinary capacities.[4,5]

When electrodes are put into contact with an electrolyte, the polar molecules and ions will induce image charges on the electrode's surface. In particular upon applying a voltage, ions are forced into the vicinity of the electrode and the ion's charge is compensated by a respective charge of opposite sign on the electrode—the electrostatic double layer is formed.[6]

While the formation of image charges[7] and interactions between liquids and electrodes[8–10] can be modeled on the nanoscale using quantum mechanical methods, such as density-functional theory or tight binding, these are limited to a couple of hundred atoms. In particular, if a large number of electrolyte molecules is to be included in the simulation, the number of atoms will exceed the possibilities of quantum-chemical methods by orders of magnitude. A proper description of electrodes hence requires an inexpensive classical method.

Such classical models have been traditionally developed for molecules[11] and dielectrics.[12] Coincidentally, these early variable-charge models use a formulation that is only strictly valid for metals (such as electrodes) since charge can transfer over arbitrary distances.[13] Indeed, such models have also been used to study the structure of water in the vicinity of charged metallic electrodes.[14,15] For dielectrics, more recent developments allow proper modeling of polarizabilities.[16]

Here we present a variable-charge model for metallic electrodes, which is similar in spirit to earlier variable-charge formulations.[11,12,14,15] We derive the respective total-energy expression from the material's electronic structure. In short, for CNTs and graphene—the two model materials considered here—the surface density of states is expressed as a compact analytical expression[2] from which a mean-field model for charge transfer is derived. Thus, whereas the Siepmann-Sprik model,[15] for instance, uses a term quadratic in the atomic charges, fitted to reproduce the proper limit of macroscopic electrostatics, our model allows penalizing charge transfer using the exact energy expressions following from the electronic structure. Physically, the Siepmann-Sprik model hence contains electrostatic interaction and a Hubbard-U term which can be regarded as contributions to the Hartree energy. Our model additionally contains a rough estimate of the electron kinetic, exchange, and correlation energies within the rigid-band approximation. The model parameters are easily extracted from these considerations without the need for empirical parametrization schemes.[12,14,15] Obviously, such a model is only appropriate for studying double-layer formation at inert electrodes at which no Faradaic processes occur.

II. THEORY

We construct this charge-transfer model starting at the quantum level. Specifically, in the tight-binding approximation[17,18] including self-consistent charges[17–19] the total energy is given by

$$E(\rho) = E^{\mathrm{BS}} + \frac{1}{2}\sum_{I,J}\gamma_{IJ}q_I q_J + \sum_I \phi_I^{\mathrm{ext}} q_I \qquad (1)$$

with $E^{\mathrm{BS}} = \mathrm{tr}\,\rho H$, the band-structure energy. Here, ρ is the density matrix, H the tight-binding Hamiltonian, q_I the total (nucleus plus electron) charge on atom I, γ_{IJ} the Coulomb integral between atoms I and J, and ϕ_I^{ext} the potential at atom I from the electrolyte molecules, including a possible external potential. The long-range tail of γ_{IJ} decays as $\gamma_{IJ} \sim r_{IJ}^{-1}$. The short-range behavior of γ_{IJ} deviates from r^{-1} which honors the fact that the electron is delocalized: the charge

located on each atom acquires some shape that broadens the point charge. In particular, the self-energy contribution is contained in γ through $\gamma_{II} = U$, where the Hubbard-U is often called the chemical hardness. In Eq. (1), we deliberately omitted the repulsive pair potential that is required to stabilize solid state structures since we only focus on the ground state of the electronic system.

An electrolyte consists of solvated ions and the solvent. We here approximate both by a set of point charges which present a spatially varying external electrostatic potential ϕ_I^{ext} to the electrode. The equilibrium density matrix ρ on the electrode can be found by minimizing Eq. (1), which yields

$$\bar{\mu} = \mu_I + \sum_J \gamma_{IJ} q_J + \phi_I^{\text{ext}} = \text{const.}, \tag{2}$$

i.e., the electrochemical potential $\bar{\mu}$ has to be constant. This minimization is constrained by the condition that ρ remains idempotent, i.e., $\rho^2 = \rho$, and that the trace of ρ gives the number of electrons in the system. The charges q_I are traces over the subspace of ρ that is localized on the respective atom.

A full solution of Eq. (2) is numerically prohibitive for more than around 1000 atoms, hence approximations need to be made to the band-structure part of the energy

$$E^{\text{BS}} = \text{tr}\,\rho H = \int_{-\infty}^{\epsilon_F} d\epsilon\, \epsilon D(\epsilon) \tag{3}$$

in order to compute the response of the system to an external electrostatic potential ϕ_I^{ext}. Here, μ is the chemical potential and $D(\epsilon)$ the electron density of states. In particular, we want the approximate energy expression to only depend on the charges q_I and the solution of the unperturbed system (where $\phi_I^{\text{ext}} = 0$), and not on the full density matrix ρ. Numerically, this reduces the dimensionality of the problem to linear order.

The band-structure energy of the unperturbed solution is fully determined by the knowledge of the density of states $D(\epsilon)$. For graphene and CNTs, which we are treating here, we know that due to symmetry the local density of states $g_I(\epsilon)$ has to be equal for each atom I, and hence equal to the unperturbed total density of states $D(\epsilon)$ (with appropriate normalization). We may hence write trivially

$$D(\epsilon) = \sum_I g_I(\epsilon) = \sum_I g(\epsilon), \tag{4}$$

with $g(\epsilon) = N^{-1} D(\epsilon)$, where N is the total number of atoms in the crystal. We now assume that the local density of states is *rigid*: An external potential will only shift the local density of states by the value μ_I of the local chemical potential. Hence,

$$D(\epsilon) = \sum_I g(\epsilon - \mu_I) \tag{5}$$

and

$$E^{\text{BS}} = \sum_I \int_{-\infty}^{\epsilon_F + \mu_I} d\epsilon\, g(\epsilon) = \sum_I e^{\text{BS}}(\mu_I), \tag{6}$$

where e^{BS} is a per-atom contribution to the band-structure energy. This rigid-band approximation[20] is the central assumption in our charge-transfer model.

In order to determine the density of states $g(\epsilon)$ we need a specific material model. A spin-paired π-orbital tight-binding Hamiltonian with a single electron per carbon atom is sufficient to describe the electron dispersion around the Fermi level for infinite CNTs and graphene.[2] In particular, we can additionally linearize the dispersion relation around the Fermi level which leads to the famous $\mathbf{k} \cdot \mathbf{p}$ Hamiltonian[21] that describes the idealized spherically symmetric Dirac-cone centered at the K points in the two-dimensional band structure of graphene. Similarly, for metallic CNTs in the zone-folding approximation the band structure becomes linear and the slope is identical to that of the graphene Dirac cone.[2]

Figure 1 shows a comparison of these approximate solutions to the solution obtained using density-functional theory (DFT).[22] In particular, Fig. 1(c) shows that the band-structure energy is faithfully reproduced close to the Fermi level. For CNTs, moving away from the Fermi-level reveals the sub-band quantization in the fully nonlinearized model (see kinks in the blue curve of Fig. 1(c)). While it is easy to also include this in the linearized model (see Ref. 23), we refrain here from doing so for the sake of simplicity. For large diameter CNTs, the graphene model again gives a reasonable approximation

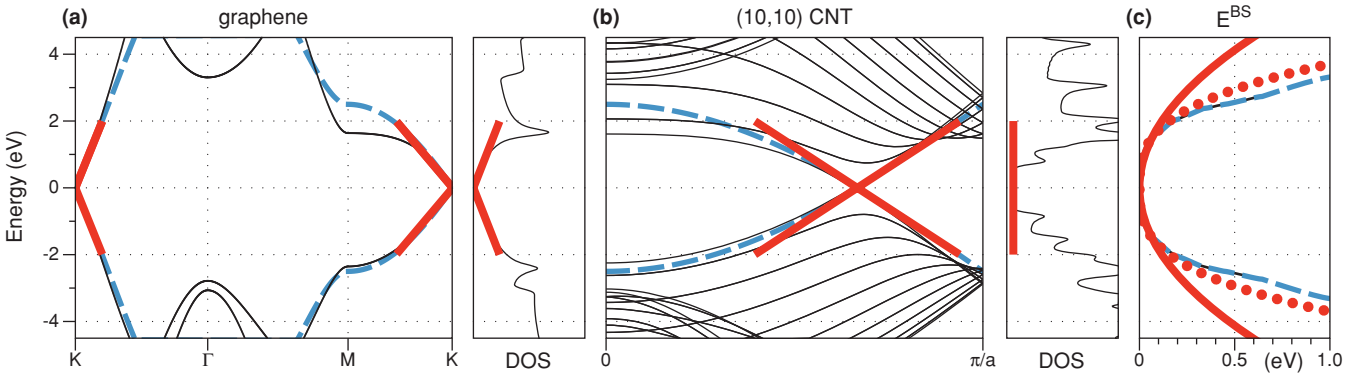

FIG. 1. (Color online) Band structure and density of states for (a) graphene and (b) a (10,10) CNT. (c) Band-structure energy E^{BS} as a function of chemical potential, where dotted lines are graphene results while solid lines give the results for a (10,10) CNT. In all graphs, the DFT-LDA solution is shown with thin (black) lines, while thick lines show the nearest-neighbor π-orbital tight-binding model with $t_0 = 2.5$ eV. Here, the dashed (blue) is the full and solid (red) the linearized solution. The kinks in the dashed lines are due to the subband quantization in the full solution. The Fermi-level is located at zero energy.

and an explicit inclusion of sub-band quantization becomes unnecessary.

The linearized band structures lead to an approximate analytical expression for the density of states, $g(\epsilon) = G|\epsilon|^{\alpha}$, with $\alpha = 0$ for metallic CNTs[23] and $\alpha = 1$ for graphene.[24] This approximation is valid close to the Fermi level which is located at $\epsilon_F = 0$. By normalizing the density of states to the number of carbon atoms, we obtain[23,24]

$$G_{\mathrm{CNT}} = \frac{4}{\pi\sqrt{n_1^2 + n_2^2 + n_1 n_2}\, t_0}, \tag{7}$$

$$G_{\mathrm{graphene}} = \frac{2}{\sqrt{3}\,\pi\, t_0^2}. \tag{8}$$

Here t_0 is the next-neighbor hopping matrix element and (n_1,n_2) the tube's chirality. Using $t_0 = 2.5\,\mathrm{eV}$ (see, e.g., Refs. 2, 20, and 23) this gives $G^{-1} = 17.0\,\mathrm{eV}^2$ for graphene. For (5,5) and (10,10) CNTs the values are 17.0 eV and 34.0 eV, respectively.

The corresponding expression for the band-structure energy per atom becomes

$$e^{\mathrm{BS}}(\mu) = e_0 + \frac{G}{\alpha+2}|\mu|^{\alpha+2}, \tag{9}$$

where $e_0 = e^{\mathrm{BS}}(\epsilon_F)$ will be omitted in the following.[25] This energy can be expressed in terms of the total net charge per atom element

$$q(\mu) = -|e| \int_{\epsilon_F}^{\mu} d\epsilon\, g(\epsilon) \tag{10}$$

leading to

$$e^{\mathrm{BS}}(q) = \frac{G}{\alpha+2}\left(\frac{\alpha+1}{G}\frac{|q|}{|e|}\right)^{\frac{\alpha+2}{\alpha+1}}. \tag{11}$$

The total band-structure energy is then given by

$$E^{\mathrm{BS}} = \frac{(\alpha+1)^{\frac{\alpha+2}{\alpha+1}}}{\alpha+2} G^{-\frac{1}{\alpha+1}} \sum_I \left(\frac{|q_I|}{|e|}\right)^{\frac{\alpha+2}{\alpha+1}} \tag{12}$$

which is now a function of the charges q_I.

To obtain the equilibrium charge distribution q_I we minimize Eq. (1) [with the approximate expression Eq. (12) for the band-structure energy] under the constraint that the total charge on the electrode is Q. Hence we need to minimize

$$\Omega(\mathbf{q}) = E(\mathbf{q}) - \bar{\mu}\left(\sum_I q_I - Q\right), \tag{13}$$

where $\Omega(\mathbf{q})$ is the grand-canonical potential, and the electrochemical potential $\bar{\mu}$ is introduced here as a Lagrange multiplier. This gives a set of equations

$$g\left(\frac{|q_I|}{|e|}\right)^{p} + \phi_I - \bar{\mu} = 0 \tag{14}$$

with $\phi_I = \sum_J \gamma_{IJ} q_J + \phi_I^{\mathrm{ext}}$ and

$$g = (pG)^{-p} \text{ and } p = \frac{1}{\alpha+1}. \tag{15}$$

Note that Eq. (14) is the equilibrium condition Eq. (2). We rewrite Eq. (14) as

$$\frac{q_I}{|e|} = -\left|\frac{\phi_I - \bar{\mu}}{g}\right|^{\frac{1}{p}} \mathrm{sgn}(\phi_I - \bar{\mu}). \tag{16}$$

In the spirit of tight-binding models, Eq. (16) is solved self-consistently for the q_I's using Anderson mixing.[26,27] In each step, we solve for the electrochemical potential $\bar{\mu}$ which gives total charge Q using a Newton iteration. Note that for nanotubes $p = 1$ and $\bar{\mu}$ can be computed directly.

At this point, we would like to emphasize a connection to the theory of interatomic bonding: Our charge-transfer model is solely based on the functional form of the local density of states. Second-moment tight-binding bond models are successful in describing bonding in d metals. Also here, the local density of states is the central quantity from which the bonding characteristics of the material can be derived.[18] While we know the exact local density of states in the unperturbed case, for these interatomic potentials Gaussians or constant values (over a range of energies) are typically assumed for $g(\epsilon)$. These functions could be easily used to derive charge-transfer models for d metals. A constant local density of states then leads to a quadratic dependence of the band-structure energy on q_I, identical to the CNT model derived here.

III. MODEL VALIDATION

Equation (12) holds only for slowly varying fields in the sense of a local-density approximation. This model hence excludes interferences due to electrons scattering at the impurity potential caused by the ion's charge which typically lead to Friedel-type charge oscillations. Equation (12) is a *mean-field* theory for the response of the respective carbon nanostructure which, however, gives the correct quantum capacity[28] of the device since the integral response to homogeneous charging is correct.

It is less obvious that the model should reproduce the limit opposite to homogeneous charging, i.e., the response to a point charge. We hence calculate the response of different systems in the vicinity of a point charge and compare to nonorthogonal tight-binding calculations (NOTB) using the parametrization of Ref. 29. In both cases, a Hubbard-U of 9.9 eV and Gaussian charges[17] are used.

Figure 2 shows the energy as a function of distance, as the point charge $q = 1|e|$ is moved from the middle of a hexagon outwards on graphene, a (10,10) and a (5,5) CNT, while the whole system is kept charge neutral. We use 2D and 1D periodicity for the graphene and the CNTs, respectively, where the repeat unit is constructed out of 8×12 rectangular graphene unit cells, and 20 CNT unit cells. For comparison, we also show the classical results that are expected in the limit of infinite separation. Because of the periodicity, the interaction energy E per surface area A approaches the interaction energy of two charged parallel plates at distance d

$$\frac{E}{A} = \frac{1}{2\varepsilon_0}\left(\frac{q}{A}\right)^2 d \tag{17}$$

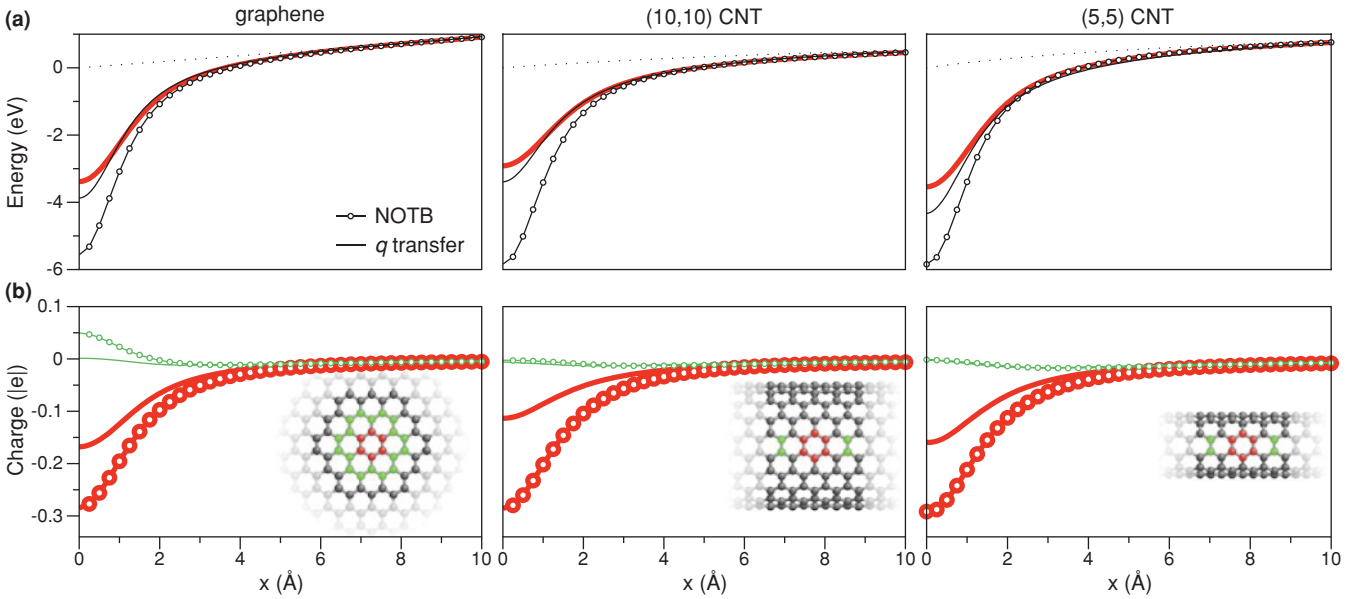

FIG. 2. (Color online) (a) Energy as a function of distance, as a point charge ($+|e|$) moves outwards from a surface hexagon of graphene, a (10,10) CNT and a (5,5) CNT (left to right). (b) Average charge on the central hexagon (thick, red) and the second-nearest neighbors (thin, green). The results are displayed for NOTB (open circles) and the charge-transfer model without the Coulomb integral (solid lines). In the top panel, the thick (red) lines give the result of the charge-transfer model including the Coulomb integral, and the dotted lines give the classical limit at large separations (see text).

for graphene, and the energy E per length L of two line charges at distance d

$$\frac{E}{L} = \frac{1}{4\pi\varepsilon_0}\left(\frac{q}{L}\right)^2 \ln d \tag{18}$$

in the case of CNTs.

In particular, the results of the charge-transfer model and NOTB agree for large distances, typically starting at around 4 Å where the error with respect to NOTB calculations drops below 0.1 eV. Remarkably, the charge-transfer results move closer to NOTB results for small separations if we only consider the self-energy contribution of the Hubbard-U and let the Coulomb integral $\gamma_{IJ} = r_{IJ}^{-1}$. The full Coulomb integral γ_{IJ} provides some smoothing of the charge oscillations in the vicinity of the impurity. With $\gamma_{IJ} = r_{IJ}^{-1}$ this smoothening is switched off, leading to more pronounced charge oscillations, a behavior closer to the Friedel oscillations observed in the NOTB model.

The agreement between NOTB and charge transfer is worst in the case of the (10,10) CNT shown in Fig. 2(b). In particular at small distances the error in binding energy is around 2.5 eV while at larger distances the proper limiting behavior is obtained. For a (10,10) CNT, the first sub-band starts around 1 eV above and below the Fermi level (see Fig. 1). The inhomogeneous response to an inducing charge closer than 4 Å will shift the local chemical potential into the sub-band region, hence explaining the observed difference. For the (5,5) tube, where the first sub-band is located around 2 eV from the Fermi level, the agreement between the charge-transfer model and NOTB calculations is better.

At aqueous solution-electrode interfaces, the ions remain at distances above 4 Å where our model gives accurate binding energies. The water itself is charge neutral, such that only dipole and higher-order electrostatic interactions play a role. In order to check the interaction of water with a charge-neutral electrode we conduct molecular dynamics simulations of a water droplet consisting of 1070 water molecules on a graphene substrate at 300 K (see Fig. 3(a)). Here, water is simulated with the SPC/E model,[30] whereas for graphene-water a C-O Lennard-Jones potential fitted to reproduce the water–graphite contact angle is used[31] ($\epsilon_{CO} = 4.06$ meV and $\sigma_{CO} = 3.19$ Å).

When equilibrating the droplet we find no observable change in contact angle with respect to the charge-neutral case, to which the Lennard-Jones potential has been fitted. To crosscheck, we also computed typical binding energies of water on graphene and a (5,5) CNT. Here, the water is oriented such that the two hydrogens point away from the surface. Binding energies are a few meV for the closest distance of around 2.5 Å which we observed in molecular dynamics simulations. This gives only a minor increase in the energy of the water–graphene interface. Thus upon introducing charge transfer, the water–graphite contact angle is preserved.

IV. WATER DROPLET IN A BIASED GRAPHENE NANOCAPACITOR

We now carry out simulations of a water droplet in a graphene nanocapacitor. This setup is similar to previous studies of water on charged surfaces.[32,33] The capacitor is constructed by adding a second graphene layer at a distance of 20 nm from the graphene on which the droplet resides (Fig. 3(a)).

We employ two methods of charging: First, we use our charge-transfer model and apply a voltage across the capacitor by adding an energy penalty term $\phi_I^{\text{ext}} = \chi_I$ for each electrode

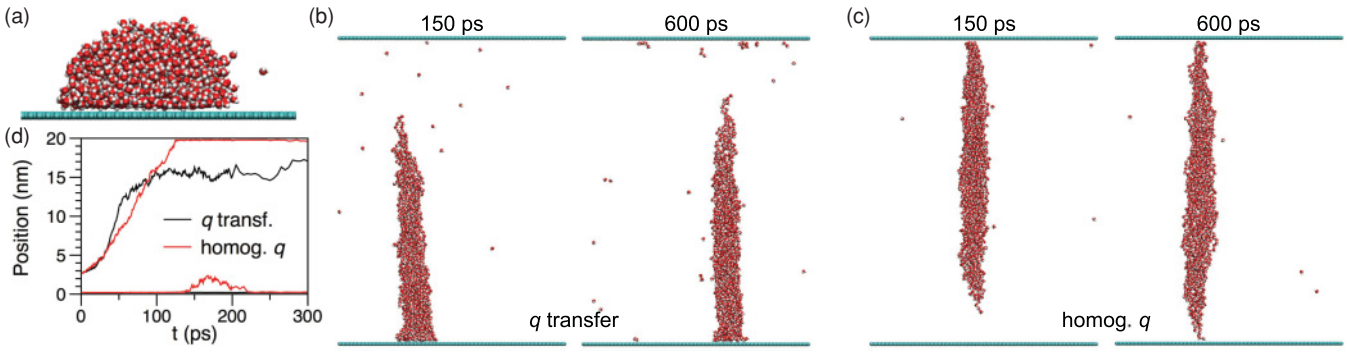

FIG. 3. (Color online) Snapshots of the droplet in the capacitor. (a) Initial configuration, (b) including charge-transfer, and (c) using homogeneous charging. (d) Position of the top- and bottommost water molecule over time after the equilibrated droplet has been placed in a capacitor setup.

atom I. Here, χ_I is constant on each capacitor plate and the difference in χ_I between the plates is the applied voltage as can be seen from Eq. (2). Second, we homogeneously charge the capacitor so that $q_I = \pm q$, the sign depending on the electrode, and the resulting field corresponding to the desired voltage.

In agreement with previous work,[32,33] the droplet elongates and forms a stable pillar-like structure between the two electrodes (Fig. 3(b) and 3(c)). Figure 3(d) shows the position of top- and bottommost water molecule in the droplet at 30 V. We see that the droplet elongates but remains on the initial graphene surface if charge is allowed to rearrange (see also Fig. 3(b)). Conversely, in the case of homogeneous charging the droplet elongates until it touches both surfaces (Fig. 3(c)). At around 150 ps it even detaches from the lower graphene electrode showing it's low tendency to adhere to the graphene.

Remarkably, the charge-transfer treatment leads to a different behavior in both contact angle and the rise velocity of the droplet. This difference in behavior between the constant- and variable-charge model is sustained over a large voltage-range. We observe the onset of pillar formation at around 15 V, while above 150 V we observe a Taylor-like instability and the single pillar decays into multiple ones.

The origin of the observed behavior is the dielectric property of the water. Since the water provides a higher dielectric constant than the vacuum, it is energetically beneficial to locate some of the charge on the electrode below the droplet. We find an average induced charge of $0.002\,|e|\,\mathrm{atom}^{-1}$, while below the droplet the average charge is roughly $0.012\,|e|\,\mathrm{atom}^{-1}$ after 600 ps.

V. CONCLUSIONS

For simulating carbonaceous nanostructures in polar environments, the present model gives energetics close to tight-binding calculations. Especially beneficial is the controlled parametrization from quantum mechanical considerations and measured- or analytical-band structures. Together with a functional form familiar from traditional charge equilibration models, this allows for a fast implementation of the model into existing molecular dynamics codes.

We demonstrate the model using a simple nanocapacitor setup. In particular, this system was deliberately chosen as simple as possible: The droplet does not contain ions since we do not intend to change the interfacial energies at zero bias as demonstrated above; the capacitor plates are parallel as to provide an initially homogeneous electric field. Still, the biased system behaves remarkably differently from the constant-charge situation.

The capacitor serves as a demonstration that a proper consideration of charge-transfer is crucial for the simulation of *biased* nanosystems. The present model will hence enable the study of double-layer formation as a function of voltage in systems such as supercapacitors with carbon nanotube forest electrodes. In this particular example, we expect non-homogeneous field distributions that are induced by the geometry of the electrodes, and hence a behavior that necessitates the use of charge-transfer models.

Although we use carbon structures as an example because analytic expressions for the densities of states are available, the model is by no means restricted to such systems. As outlined in Sec. II, similar approximate charge-transfer models can be derived for any kind of metallic material.

ACKNOWLEDGMENTS

This work was funded by the Fraunhofer Society (MaVo "CarNAk"), the German Federal Ministry of Education and Research (projects "KoLiWIn"/03SF0343G and "MALION"/13N10599), and the Academy of Finland (project no. 136165).

*tommi.jarvi@iki.fi

[1] E. Frackowiak, Phys. Chem. Chem. Phys. **9**, 1774 (2007).
[2] R. Saito, G. Dresselhaus, and M. S. Dresselhaus, *Physical Properties of Carbon Nanotubes* (Imperial College Press, London, 1998).
[3] A. K. Geim, Science **324**, 1530 (2009).
[4] M. D. Stoller, S. Park, Y. Zhu, J. An, and R. S. Ruoff, Nano Lett. **8**, 3498 (2008).
[5] C. Liu, Z. Yu, D. Neff, A. Zhamu, and B. Z. Jang, Nano Lett. **10**, 4863 (2010).
[6] H.-J. Butt, K. Graf, and M. Kappl, *Physics and Chemistry of Interfaces* (Wiley-VCH, Berlin, 2003).

[7] P. Pomorski, L. Pastewka, C. Roland, H. Guo, and J. Wang, Phys. Rev. B **69**, 115418 (2004).
[8] G. Cicero, J. C. Grossman, E. Schwegler, F. Gygi, and G. Galli, J. Am. Chem. Soc. **130**, 1871 (2008).
[9] F. Schiffmann, J. Hutter, and J. VandeVondele, J. Phys. Condens. Matter **20**, 064206 (2008).
[10] K. Leung and J. L. Budzien, Phys. Chem. Chem. Phys. **12**, 6583 (2010).
[11] A. K. Rappé and W. A. Goddard III, J. Phys. Chem. **95**, 3358 (1991).
[12] F. H. Streitz and J. W. Mintmire, Phys. Rev. B **50**, 11996 (1994).
[13] T. Verstraelen, V. V. Speybroeck, and M. Waroquier, J. Chem. Phys. **131**, 044127 (2009).
[14] M. Pounds, S. Tazi, M. Salanne, and P. A. Madden, J. Phys. Condens. Matter **21** (2009).
[15] J. I. Siepmann and M. Sprik, J. Chem. Phys. **102**, 511 (1995).
[16] R. A. Nistor, J. G. Polihronov, M. H. Müser, and N. J. Mosey, J. Chem. Phys. **125**, 094108 (2006).
[17] P. Koskinen and V. Mäkinen, Comput. Mater. Sci. **47**, 237 (2009).
[18] M. W. Finnis, *Interatomic Forces in Condensed Matter* (Oxford University Press, Oxford, 2004).
[19] M. Elstner, D. Porezag, G. Jungnickel, J. Elsner, M. Haugk, T. Frauenheim, S. Suhai, and G. Seifert, Phys. Rev. B **58**, 7260 (1998).
[20] L. Pastewka, P. Koskinen, C. Elsässer, and M. Moseler, Phys. Rev. B **80**, 155428 (2009).
[21] D. P. DiVincenzo and E. J. Mele, Phys. Rev. B **29**, 1685 (1984).
[22] We use the local-density approximation[34] in combination with the projector augmented wave method[35] on a real-space grid[36] with a spacing of $h = 0.20$.
[23] J. W. Mintmire and C. T. White, Phys. Rev. Lett. **81**, 2506 (1998).
[24] A. H. C. Neto, F. Guinea, N. M. R. Peres, K. S. Novoselov, and A. K. Geim, Rev. Mod. Phys. **81**, 109 (2009).
[25] Note that while in a nearest-neighbor model $\epsilon_F = 0$, this is lifted already when including next-nearest neighbors. Generally, $\epsilon_F \neq 0$ leads to a term linear in μ in Eq. (9). Charge conservation removes this term unless different atomic species with different electronegativities are considered.
[26] V. Eyert, J. Comput. Phys. **124**, 271 (1996).
[27] This scheme has been implemented in a customized version of the molecular dynamics code LAMMPS.[37]
[28] M. Büttiker, J. Phys. Condens. Matter **5**, 9361 (1993).
[29] D. Porezag, T. Frauenheim, T. Köhler, G. Seifert, and R. Kaschner, Phys. Rev. B **51**, 12947 (1995).
[30] H. J. C. Berendsen, J. R. Grigera, and T. P. Straatsma, J. Phys. Chem. **91**, 6269 (1987).
[31] T. Werder, J. H. Walther, R. L. Jaffe, T. Halicioglu, and P. Koumoutsakos, J. Phys. Chem. B **107**, 1345 (2003).
[32] T. Cramer, F. Zerbetto, and R. García, Langmuir **24**, 6116 (2008).
[33] C. D. Daub, D. Bratko, K. Leung, and A. Luzar, J. Phys. Chem. C **111**, 505 (2007).
[34] J. P. Perdew and A. Zunger, Phys. Rev. B **23**, 5048 (1981).
[35] P. E. Blöchl, Phys. Rev. B **50**, 17953 (1994).
[36] J. J. Mortensen, L. B. Hansen, and K. W. Jacobsen, Phys. Rev. B **71**, 035109 (2005).
[37] S. Plimpton, J. Comput. Phys. **117**, 1 (1995), LAMMPS is available at [http://lammps.sandia.gov].